

ORIGINAL RESEARCH

Open Access



Biological efficacy of simulated radiolabeled Lipiodol[®] ultra-fluid and microspheres for various beta emitters: study based on VX2 tumors

Arnaud Dieudonné^{1,2*} , Stéphanie Becker^{1,2}, Miguel Soares³, Claire Hollenbeck³, Marie-Christine De Goltstein³, Pierre Vera^{1,2} and Robin Santus³

Abstract

Background Radioembolization is one therapeutic option for the treatment of locally early-stage hepatocellular carcinoma. The aim of this study was to evaluate the distribution of Lipiodol[®] ultra-fluid and microspheres and to simulate their effectiveness with different beta emitters (⁹⁰Y, ¹⁸⁸Re, ³²P, ¹⁶⁶Ho, ¹³¹I, and ¹⁷⁷Lu) on VX2 tumors implanted in the liver of 30 New Zealand rabbits.

Results Twenty-three out of 30 rabbits had exploitable data: 14 in the group that received Lipiodol[®] ultra-fluid (group L), 6 in the group that received microspheres (group M), and 3 in the control group (group C). The histologic analysis showed that the Lipiodol[®] ultra-fluid distributes homogeneously in the tumor up to 12 days after injection. The X-ray μ CT images showed that Lipiodol[®] ultra-fluid has a more distal penetration in the tumor than microspheres. The entropy (disorder of the system) in the L group was significantly higher than in the M group (4.06 vs 2.67, $p=0.01$). Equivalent uniform biological effective doses (EUBED) for a tumor-absorbed dose of 100 Gy were greater in the L group but without statistical significance except for ¹⁷⁷Lu ($p=0.03$). The radionuclides ranking by EUBED (from high to low) was ⁹⁰Y, ¹⁸⁸Re, ³²P, ¹⁶⁶Ho, ¹³¹I, and ¹⁷⁷Lu.

Conclusions This study showed a higher ability of Lipiodol[®] ultra-fluid to penetrate the tumor that translated into a higher EUBED. This study confirms ⁹⁰Y as a good candidate for radioembolization, although ³²P, ¹⁶⁶Ho, and ¹⁸⁸Re can achieve similar results.

Keywords VX2, Dosimetry, SIRT, Lipiodol, Microspheres

Background

Hepatocellular carcinoma (HCC) is the most common primary liver cancer that develops from liver cells. It is the seventh most common cause of cancer worldwide and the second most common cause of cancer death [1]. Many treatments are used (from surgery to palliative treatment), selected according to the BCLC (Barcelona Clinic Liver Cancer) recommendations. Radioembolization is one option for treatment that has recently been introduced in the BCLC classification for early-stage patients [2].

*Correspondence:

Arnaud Dieudonné
arnaud.dieudonne@me.com

¹ Nuclear Medicine Department, Henri Becquerel Cancer Center, 76000 Rouen, France

² QuantIF-LITIS EA4108, University of Rouen, Rouen, France

³ Research and Development Division, Laboratoire Guerbet, Aulnay-Sous-Bois, France

The products currently approved for clinical use are glass microspheres (TheraSphere[®], Boston Scientific), resin microspheres (SIR-Sphere[®], SIRTEX Medical), both labeled with yttrium-90 (⁹⁰Y), and polyglycolic acid-co-dl-lactic acid (PGLA) microspheres labeled with holmium-166 (¹⁶⁶Ho) (QuiremSpheres[™], Terumo). The physicochemical characteristics of these different microspheres vary very slightly in diameter, but their main difference is their range of activity per microsphere, which is summarized in Table 1.

The quantity of microspheres injected varies according to the activity to deliver and the calibration of the delivered vial. Indeed, TheraSphere[®] can be injected with varying activity per sphere, from a maximum of 2500 Bq per microsphere at the time of calibration, down to 70 Bq at the expiration date (15 days after calibration). For SIR-Spheres[®], the activity per vial orderable is between 3 and 10 GBq with a fixed number of microspheres, which leads to an activity per sphere between 50 and 150 Bq. This results in different biodistributions, which were described in the liver parenchyma [3] and impacts the acceptable dose limit in the healthy liver [3–5]. The impact on the tumor is also suspected to result in a different dose–response profile according to the microsphere load as suggested by Romanò et al. [6].

An alternative to the use of microspheres is to inject radiolabeled Lipiodol[®] ultra-fluid. This method was originally developed with Iodine-131 (¹³¹I) [7, 8] and was commercially available in the 2000s as Lipiocis[®] (CIS BIO International, Gif-Sur-Yvette, France). Radiolabeling of Lipiodol[®]

ultra-fluid was also proposed with a rhenium-containing ligand dissolved in Lipiodol[®] ultra-fluid, the complex SSS, which stands for “Super-Six sulfur”. A Lipiodol[®] labeled with rhenium-188 (¹⁸⁸Re) has been proposed [9].

The benefit of Lipiodol[®] ultra-fluid is that its biodistribution in the hepatic tumor has been described for years in the context of trans-arterial embolization. Its penetration to the venous sinuses, its extravasation, and its intracellular internalization give it a very high tumor coverage [10, 11]. The accumulation of Lipiodol[®] ultra-fluid in the tumor results from the specific characteristics of the tumor microenvironment described by Folkman [12]. The lack of contractility of the neovessel, the very slow blood flow [13, 14], and the increase in vascular permeability lead to an accumulation in the extracellular space.

Several radionuclides have been selected as candidates for radioembolization with Lipiodol[®] ultra-fluid [15] and are summarized in Table 2. They are all beta emitters and have a relatively long half-life (> 10 h). The value Δ_β/λ is the ratio of Δ_β the average energy released per β disintegration and λ the physical decay constant of the radionuclide, which stands as the total energy releasable for a source of 1 Bq. For a given radionuclide, the β radiation-absorbed dose D_β can be calculated according to this value, with the assumption of low penetrating particles and high retention over time:

$$D_\beta = \frac{\Delta_\beta/\lambda \times A}{m} \tag{1}$$

Table 1 Characteristics of products based on radioactive microspheres available in Europe for the treatment of liver tumors as of the first quarter of 2023

	TheraSpheres [®]	SIR-Spheres [®]	QuiremSpheres [®]
Microsphere diameter	15–35 μm	20–60 μm	15–60 μm
Material	Glass	Resin	Poly(glycolic acid-co-dl-lactic acid)
Isotope	Yttrium-90	Yttrium-90	Holmium-166
Activity per microsphere	70–2500 Bq	50–150 Bq	450 Bq
Approved area	Asia, Australia, Canada, Europe, USA		Europe

Table 2 Radionuclides characteristics used in SIRT, data taken from [16] and NIST ESTAR Program [17]

	Physical half-life (h)	β released energy per disintegration Δ and CSDA range in water in parenthesis	Δ_β/λ [10^{-9} J·Bq ⁻¹]
Phosphorus-32 (³² P)	343	696 keV (2.8 mm)	198
Yttrium-90 (⁹⁰ Y)	64	933 keV (4 mm)	49.6
IODINE-131 (¹³¹ I)	192	182 keV (0.4 mm)	29.0
Holmium-166 (¹⁶⁶ Ho)	27	665 keV (2.6 mm)	14.9
Lutetium-177 (¹⁷⁷ Lu)	160	451 keV (1.5 mm)	59.8
Rhenium-188 (¹⁸⁸ Re)	17	762 keV (3.1 mm)	10.8

with A being the activity administered in the target and m the mass of the target. Depending on the radionuclide, the activity leading to a given absorbed dose can go from 1 to 20-fold (see Table 2). In addition, the continuous slowing-down approximation (CSDA), i.e., the range of the β particles goes from 0.4 to 4 mm. These differences can have an impact on therapeutic effect. Indeed, for a given average absorbed dose, differences in the micro-scale absorbed dose distribution can cause variations in the anti-tumor effect.

We propose to study these effects according to the radioembolization agent type and radionuclide using dosimetry and radiobiological modeling, to consider micro-scale heterogeneities and dose-rate effects. To this aim, we compared the biodistribution of Lipiodol® ultra-fluid with those of microspheres comparable in the rabbit hepatocarcinoma model (VX2). For each explant, the dosimetry was modeled for the following radionuclides: ^{32}P , ^{90}Y , ^{131}I , ^{166}Ho , ^{177}Lu , and ^{188}Re .

Materials and methods

Animals

All animal experiments were conducted in compliance with European Union Directive 2010/63/EU on the protection of animals used for scientific purposes. The protocol was approved by the local animal research ethics committee. All surgeries were performed under general anesthesia and aseptic conditions and were supplemented by appropriate analgesic programs.

The VX2 rabbit tumor is a commonly used animal model for translational research on HCC in interventional radiology [18]. Implantation of a VX2 fragment was performed in healthy New Zealand white rabbits (Charles River Laboratories, Saint-Germain-Nuelles, France).

VX2 well-vascularized tumor fragments (25 mg) were sampled from a carrier animal and immediately implanted in the left median lobe of the exposed liver of the recipient rabbits. One donor was used for 3–6 receivers. Tumor growth lasted at least 19 days after implantation. Ultrasound imaging was performed to ensure that the tumor had reached a length of at least 10 mm (major axis); otherwise, the animal was kept until the tumor was workable. Nineteen to twenty days after tumor induction, the population was divided into 3 groups: L for Lipiodol®, M for microspheres, and C for control.

Interventional procedure

The rabbits of the L and M groups received buprenorphine (Buprecare® 0.14 mL/kg) 1 h before surgery and were hydrated with 50 mL of saline subcutaneously in the flank. Then, they received an intravenous injection of heparin diluted to 1/10 at a dose of 50 IU/kg in the

ear. A pediatric valve introducer 4F (Radifocus® TER-UMO™) was inserted into the femoral vein and a 1.7F catheter (Microcatheter 1.7F angle 90° - ECHELON™ - MEDTRONIC EV3) was guided under x-ray angiography (Philips Veradius®) to the feeding artery of the tumor at the level of the left hepatic artery. After removal of the catheter, the skin and muscle planes were sutured at the paw level.

Injection

The L group received an adjusted dose of Lipiodol® ultra-fluid into the left common hepatic artery up to reflux or pulmonary passage and to a maximum volume of 0.4 mL. The Lipiodol® ultra-fluid (Guerbet) injection liquid contains per 1 ampoule of 10 mL ethyl esters of iodized fatty acids of poppy seed oil, equivalent to 4.8 g of iodine (480 mgI/mL).

The M group received a fixed volume of 0.3 mL of microspheres in the same injection site. The radiopaque microspheres used in this study were made polyethylene glycol methacrylate (PEGMA) resin microspheres and were sieved to obtain an average diameter of 33 μm . They were made by Guerbet Research representative of approved microspheres in terms of size, which have been customized to make them radiopaque for the purpose of the study. Just before injection, 300 μL of microspheres were taken from the vial and suspended in 3 mL of saline water. The total amount of this suspension was injected slowly (about 0.1 mL·min⁻¹).

The C group received nothing.

Imaging

Different time intervals were studied to investigate the distribution kinetics of the products. Because of its ability to extravasate leading to a possible modification of distribution during the first hours after injection, the pharmacokinetics of Lipiodol® ultra-fluid (L group) was studied at different timepoints (15 min (D0), 1, 2, 6, 9 and 12 days). For microspheres (M group) which are known to stay several months in the intravascular compartment, only the following delays were studied: 15 min (D0) and 12 days (D12) after injection. The C group was imaged at 15 min, 6 days, and 9 days. At studied time-points, the rabbits were euthanized by an intravenous injection of pentobarbital at a dose of 1 mL/kg under general anesthesia. The liver was explanted, and the tumor was isolated for high resolution 3D X-ray micro-computerized tomography (μCT). A Quantum GX2 (Perkin-Elmer) was used with the following parameters 90 kV, 88 μA , and a CuAl filter, and an acquisition time of 14 min. The field of view diameter was 72 mm or 86 mm depending on the size of the tumor, leading to a voxel side of 0.144 mm or 0.172 mm.

Histology

For the L group, as soon as the μ CT image was acquired, the tumor was cut into slices of up to one centimeter, frozen ($- 80$ °C) and sent for analysis to Oncovet Clinical Research (Clinical Research, Loos, France). Frozen samples of liver with tumor were cut into sections of $12 \mu\text{m}$ thick. The sections were stained with Hemalum-Eosin after a previous silver staining (2.5%, 60 min, 4 °C) allowing the detection of Lipiodol[®] ultra-fluid. Assessments from the resulting histologic slides were performed by a veterinary pathologist blinded to sample. The Lipiodol[®] ultra-fluid and microspheres distributions were studied in the vascular network and in the parenchyma of the tumors.

Imaging analysis

To compare Lipiodol[®] ultra-fluid and microspheres capabilities to penetrate into tumor tissues, we applied a set of first-order radiomic features on the μ CT images. To do so, the tumors were segmented manually using the software tool 3DSlicer [19]. The radiomics features were extracted using the SlicerRadiomics extension based on PyRadiomics [20]. A Spearman correlation test was done between time delay, tumor volume, and each radiomic feature. For these variables, the 3 groups were compared using the non-parametric Wilcoxon test. The statistical significance was considered to be achieved for a p value below 0.05.

Dosimetry

Tri-dimensional (3D) dosimetry was modeled based on the Lipiodol[®] and microspheres distribution deduced from the μ CT images. The tumor contours previously defined for the radiomic analysis were used. The distribution volume of iodine was segmented by manual thresholding. All voxels belonging to this structure were scaled so that the values were ranging from 0 to 1. The resulting image templates were then used to generate the activity maps so that the total activity within the tumors was equal to 1 MBq.

The activity in voxels was converted to time-integrated activity, which is also referred as the total number of disintegrations over the course of the treatment. In radioembolization, the calculation is simplified by the fact that the biological half-life is far greater than the physical half-life of the radionuclides used. Thus, time-integrated activity $\tilde{A}(s)$ in each source voxels was calculated as

$$\tilde{A}(s) = \frac{A(s, t = 0)}{\lambda} \tag{2}$$

with $A(s, t=0)$ being the initial activity in the voxel and λ the decay constant of the radionuclide.

The absorbed dose was calculated in water using dose-point kernel (DPK) convolution implemented in a previous study [21, 22]. Water DPKs had a resolution of 0.1 mm. The dose $D(x)$ at position x was calculated as

$$D(x) = \iiint \tilde{A}(s)k_w(|s - x|)ds \tag{3}$$

with s being the position of the source, $\tilde{A}(s)$ the time-integrated activity, and k_w the kernel in water.

The absorbed dose by tumor was calculated for each radionuclide in Gy per MBq administered to the tumor, which equals the ratio of S factor over the radionuclide decay constant λ . Indeed, according to the medical internal radiation dose (MIRD) formalism [23, p. 21], the tumor-absorbed dose is expressed as:

$$D = \tilde{A} \times S \tag{4}$$

Hence, knowing that for radioembolization $\tilde{A} = \frac{A}{\lambda}$, the tumor absorbed dose over the administered activity within the tumor can expressed as:

$$\frac{D}{A} = \frac{S}{\lambda} \tag{5}$$

To compare the biological efficacy between absorbed dose distributions, the biological effective dose (BED) was calculated according to the linear-quadratic model applied to radioembolization [24] as:

$$\text{BED} = D \left(1 + \frac{\lambda}{\lambda + \mu} \times \frac{1}{\alpha/\beta} \times D \right) \tag{6}$$

with μ the DNA repair constant, α and β are the linear and quadratic cell killing constants. We set the value of μ to 0.46 h^{-1} as reported by Cremonesi et al. for tumors [25], and α and β values to, respectively, 0.037 Gy^{-1} and 0.0028 Gy^{-2} , as reported by van Leeuwen et al. [26].

To consider the heterogeneity of absorbed dose distribution, we implemented the equivalent uniform dose (EUD) concept of Jones and Hoban [27] to the BED leading to the EUBED:

$$\text{EUBED} = -\frac{1}{\alpha} \ln \left(\sum_{i=1}^N e^{-\alpha \times \text{BED}_i} \times v_i \right) \tag{7}$$

with BED_i being the histogram i th bin, v_i the volume fraction, and N the number of histogram bins. EUBEDs were calculated for absorbed doses ranging from 1 to 1000.

Statistics

Mean and standard deviation were calculated for the following variables for each radionuclide: tumor volume

V, S/λ, EUBED(D=100 Gy). The L and M groups were compared for each variable using the Kruskal–Wallis test by ranks. The statistical significance was set for a *p* value <0.05. All statistics and graphics were processed using RStudio 2022.12.0.353 [28] and R 4.2.2 [29].

Results

Population

Thirty female New Zealand rabbits were included in the study (mean body weight 3.68±0.35 kg), 19 in the Lipiodol® ultra-fluid group, 8 in the microspheres group, and 3 in the control group. Five animals were excluded from the L group due to: motion artifacts during imaging (1), sub-optimal image quality (1), tumor filling failure embolization, and highly necrotic tumor (3). Two animals were excluded from the M group due to a technical issue during injection.

Histology

The distribution kinetic of the L group shows that between 24 h and 12 days post-injection, the contrast remains homogeneously distributed in the hepatic portal zones, inside vascular structures of the tumoral capsule, and inside tumors, mainly in their peripheral stroma. Nevertheless, at 15 min post-injection, the distribution of Lipiodol® ultra-fluid appeared to be essentially

intravascular for two rabbits (J49598/K23002) and partially intravascular for one rabbit (K06029), before the product extravasates at subsequent times. As expected, microspheres always remained purely intravascular at 15 min and 12 days. Histology images results are shown in Fig. 1.

Imaging/radiomics

The analysis of the CT images allows for visual differentiation of the 2 groups: the L group presents higher density, not only in the large vessels, but also in the smaller structures and extravasated to fill the entire tumor parenchyma (except the central zone considered as necrotic), as can be seen in Fig. 2. In the M group, only large and mostly peripheral vessels showed contrast and penetration distal to the feeding vessels. This also translates into the entropy being significantly higher for the L group than for the M group (4.06 vs 2.67, *p*=0.01).

Tumor volumes were 8.73±8.0 mL for L group, 8.43±8.1 for the M group, and 15.6±2.9 mL for the C group (*p*=0.26). The time delay between injection and imaging was 3.43±4.1 days for L, 6.0±6.6 for M, and 0.0±0.6 for C (*p*=0.64). A strong negative correlation was found between entropy and time for the M group (*r*=- 0.878, *p*<0.05). The analysis of the radiomics results is presented in Fig. 3. Additional radiomic results are available as Additional file 1.

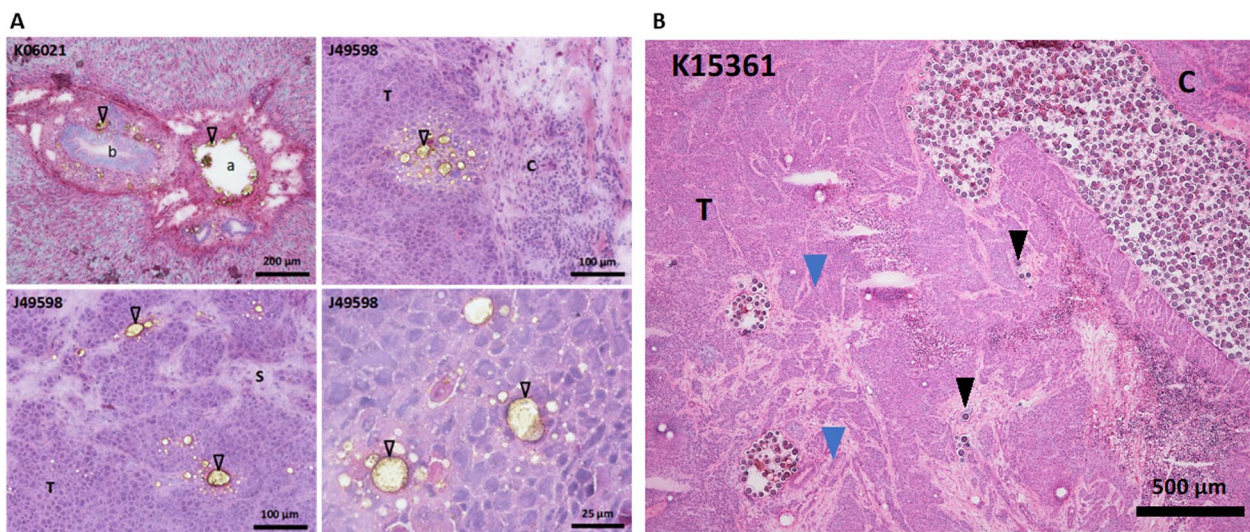


Fig. 1 Histological analysis. **A** (group L): Stainable material was present in liver portal area, both inside main (a) and smaller portal vessels (open arrowhead). Biliary canal was indicated (b). Inside the tumor, some stainable material was present at the tumor periphery near the capsule (c) as clusters of irregularly sized stainable material-containing vacuoles and in the vicinity of larger tumor stromal trabeculae (s) identified due to their lower cellular content and lighter eosinophilic stain. **B** (group M): Cluster of microspheres filling the lumen of the main arteries (blue arrow) and isolated microspheres in small capillaries inside the tumor (black arrowhead)

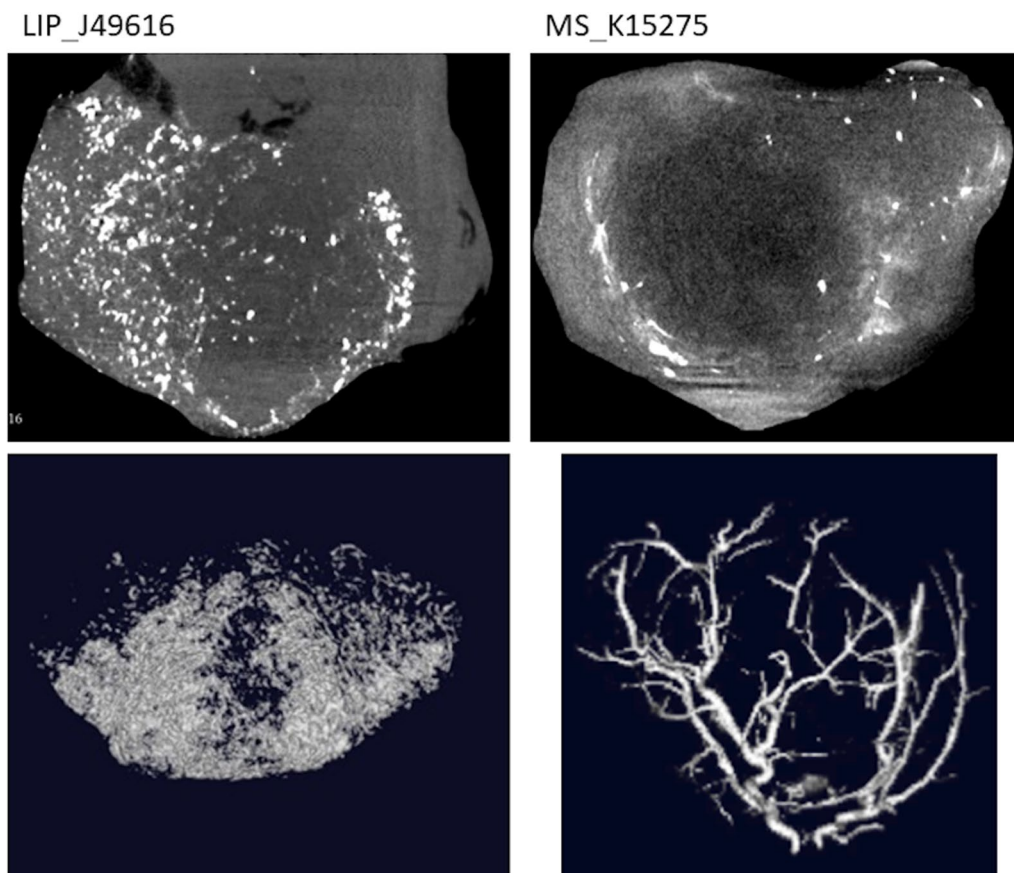


Fig. 2 Transaxial slices (top) and 3D reconstruction of iodine signal (bottom) of tumors J49616 (left) that received Lipiodol® ultra-fluid (L group) and K15275 (right) that received microspheres (M group)

Dosimetry

Figure 4 illustrates the absorbed dose maps calculated for tumors of L group and M group. The average S/λ values are 30% to 40% greater for the M group compared to the L group, but without significance: the greater hypothesis with the Wilcoxon test resulted in p values from 0.82 to 1.0. The results are presented as boxplots in Fig. 5, where one can see clearly the significantly greater S/λ values obtained for ^{32}P compared to other radionuclides in the L and M groups. As an example, for ^{32}P , $S/\lambda = 63 \pm 94 \text{ Gy}\cdot\text{MBq}^{-1}$ and $86 \pm 127 \text{ Gy}\cdot\text{MBq}^{-1}$ and for ^{90}Y , $S/\lambda = 15 \pm 22 \text{ Gy}\cdot\text{MBq}^{-1}$ and $20 \pm 29 \text{ Gy}\cdot\text{MBq}^{-1}$ in the L and M groups, respectively. Interestingly, the S/λ values of ^{90}Y are not statistically different from those of ^{131}I , despite the difference in Δ_p/λ as reported in Table 2. No statistical difference was found between ^{166}Ho , ^{177}Lu , and ^{188}Re . All S/λ data are available as Additional file 1.

Figure 6 shows the variation of EUBED as a function of the absorbed dose (D). One can see that the EUBED values tend to be much lower for ^{131}I and ^{177}Lu compared

to other radionuclides. For some tumors, the relationship between D and EUBED becomes linear over a value of D that depends on the radionuclide. It can be noted that 3 of 14 tumors of the L group curves are above the ones belonging to M group, which indicates a sign for the EUBED of the L group to be greater than that of the M group.

Indeed, average EUBED values for $D=100 \text{ Gy}$ were higher for the L group (no statistical significance) except for ^{177}Lu ($p=0.03$), see Table 3. The highest average EUBED was obtained for ^{90}Y with $45 \pm 20 \text{ Gy}$ in the L group and $37 \pm 15 \text{ Gy}$ in the M group. The lowest values were obtained for ^{131}I and ^{177}Lu with, respectively, $18 \pm 9 \text{ Gy}$ and 12 ± 7 in the L group and $9.0 \pm 4.8 \text{ Gy}$ and 5.6 ± 3.0 in the M group. In between, the EUBED values of ^{32}P , ^{166}Ho , ^{188}Re were not statistically different with, respectively, $37 \pm 16 \text{ Gy}$, $36 \pm 16 \text{ Gy}$ and $40 \pm 18 \text{ Gy}$ in the L group and $28 \pm 12 \text{ Gy}$, $27 \pm 12 \text{ Gy}$ and $31 \pm 13 \text{ Gy}$ in the M group. The comparative results between radionuclides are presented as boxplots in Fig. 7.

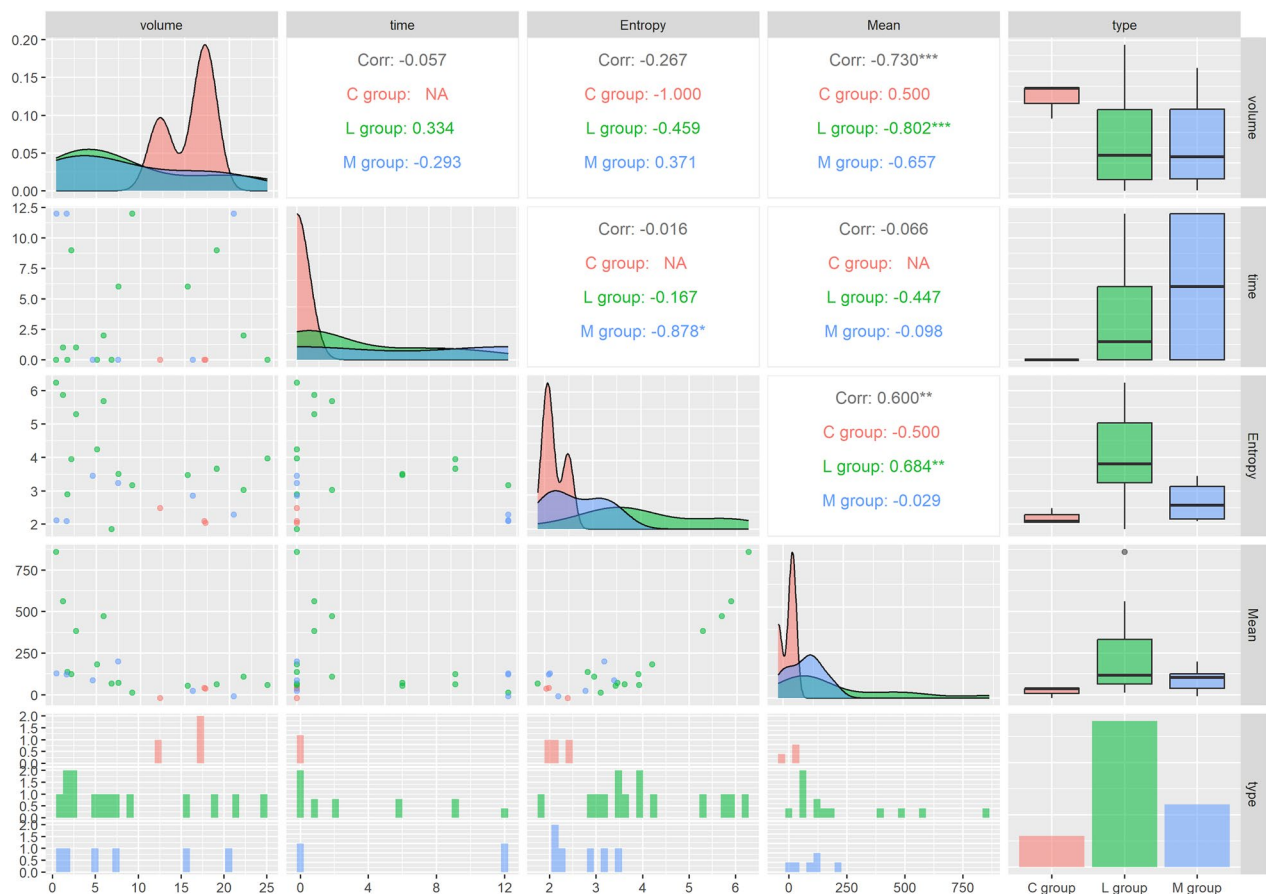


Fig. 3 Density plots, scatter plots, boxplots, and correlation (spearman) for volume, time, entropy, and mean. The number of * symbols in superscript indicates the significance of the correlation value

Discussion

Radioembolization of liver tumors is a well-established treatment strategy for HCC [2]. Currently, there are 3 major options that are based on microspheres [30]: ⁹⁰Y-resin-microspheres, ⁹⁰Y-glass-microspheres, and ¹⁶⁶Ho-PLGA-microspheres. As reported by Bouvry et al. [15], other compounds based on Lipiodol® ultra-fluid were developed and evaluated, but to date no direct comparison is available in terms of biodistribution and dosimetry.

This study aimed at comparing the biodistributions of Lipiodol® and microspheres in a VX2 tumor model implanted in rabbits. The biodistributions were assessed through histology and μCT, and absorbed dose distributions were simulated for radionuclides of interest in radioembolization, i.e., ³²P, ⁹⁰Y, ¹³¹I, ¹⁶⁶Ho, ¹⁷⁷Lu, and ¹⁸⁸Re. The distributions were analyzed visually and using first-order radiomics, while the absorbed dose distributions were completed by radiobiological modeling to compare biological effective dose (BED).

The analysis of the μCT images showed that the Lipiodol® ultra-fluid perfused the large and small vessels, feeding the tumor parenchyma but also diffuses in the extravascular compartment, while the microspheres stay strictly intravascular. This observation of Lipiodol® ultra-fluid being a more penetrative agent (confirmed by the histology) was consistent with the radiomic analysis showing a significantly greater entropy in the Lipiodol® ultra-fluid group (4.06, *n* = 14) compared to the microspheres (2.67, *n* = 6).

The dosimetry analysis showed that the absorbed dose per activity administered to the tumor (*S*/*λ*) was higher for the M group than for the L group, but without statistical significance. The highest average values were found for ³²P with 86.3 Gy·MBq⁻¹ in M group and 62.8 Gy·MBq⁻¹ in L group, which was significantly higher than ⁹⁰Y with 19.9 Gy·MBq⁻¹ and 14.9 Gy·MBq⁻¹, respectively. All other radionuclide *S*/*λ* values were below that of ⁹⁰Y. The lowest values were found for ¹⁸⁸Re with 4.67 Gy·MBq⁻¹ and 3.43 Gy·MBq⁻¹ for M and L groups, respectively.

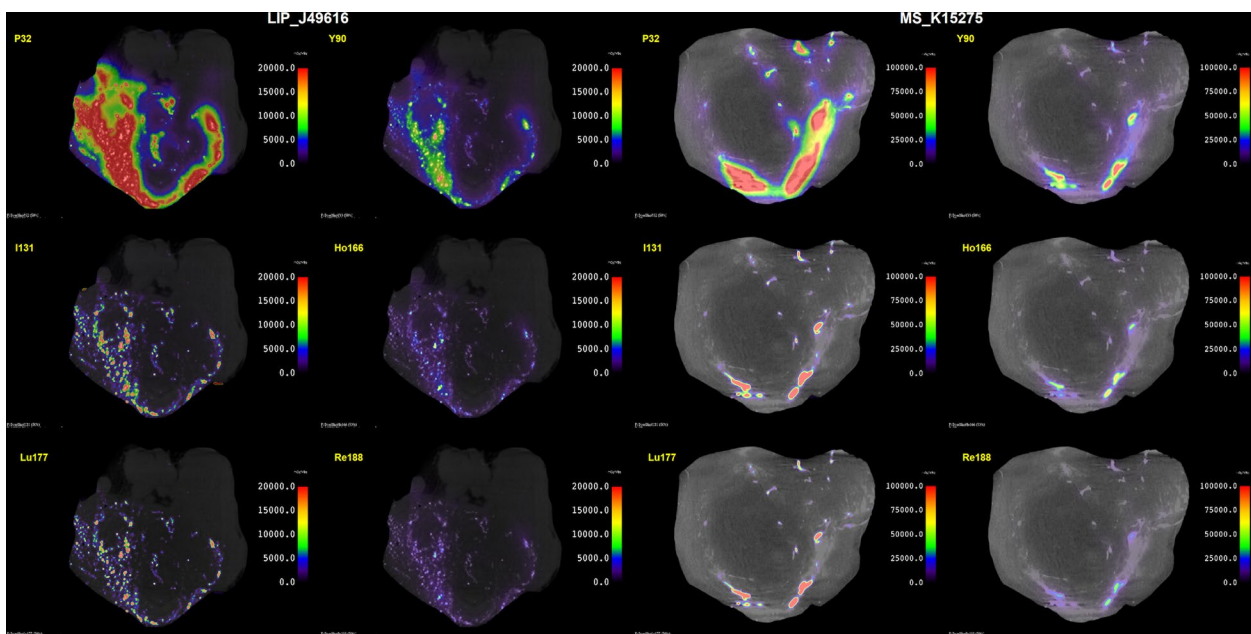


Fig. 4 Absorbed dose maps per unit of activity administered to the tumor (S/λ) in $\text{mGy}\cdot\text{MBq}^{-1}$ for ^{32}P , ^{90}Y , ^{131}I , ^{166}Ho , ^{177}Lu , and ^{188}Re in tumors LIP_J49616 (left) and MS_K15275 (right)

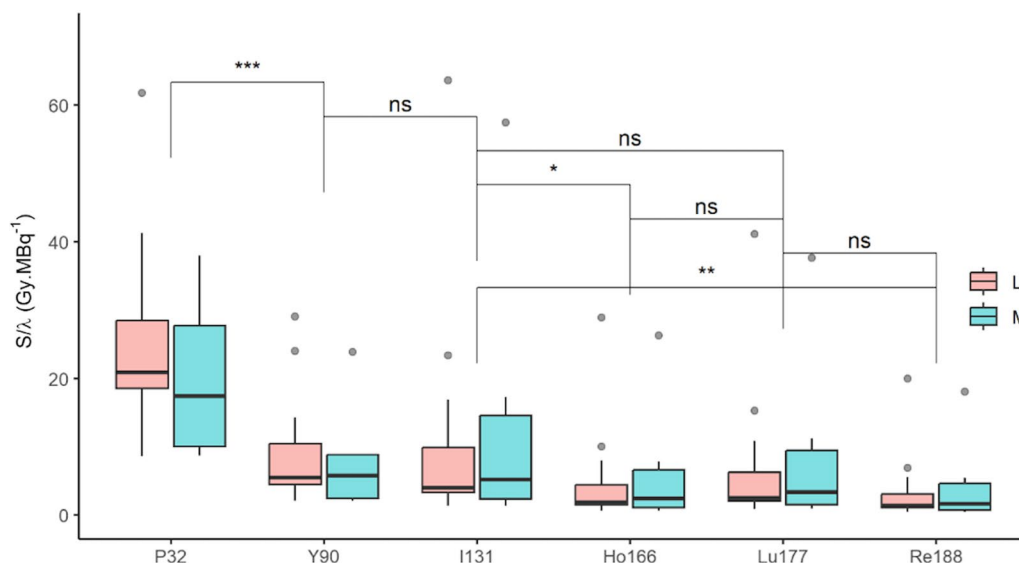


Fig. 5 S/λ in $\text{Gy}\cdot\text{MBq}^{-1}$ results presented as boxplots for the L and M groups, for ^{32}P , ^{90}Y , ^{131}I , ^{166}Ho , ^{177}Lu and ^{188}Re . *Indicates the difference is significant, while ns indicates it is non-significant

In order to simulate the biological efficacy of radionuclides, we calculated the equivalent uniform biological effective dose (EUBED), using radiobiological parameters found in the literature. The values of α and β were issued from clinical data [26]. We found that the mean EUBED values for a tumor-absorbed dose of 100 Gy were systematically higher for the L group than for the M group.

This suggests that the more distal penetration of Lipiodol® ultra-fluid should have an impact on tumor treatment efficacy, which may be expected superior to that of microspheres. Regarding the comparison between radionuclides, EUBED values were significantly higher for ^{90}Y than all other radionuclides but ^{188}Re . The lowest EUBED values were found for ^{131}I and ^{177}Lu .

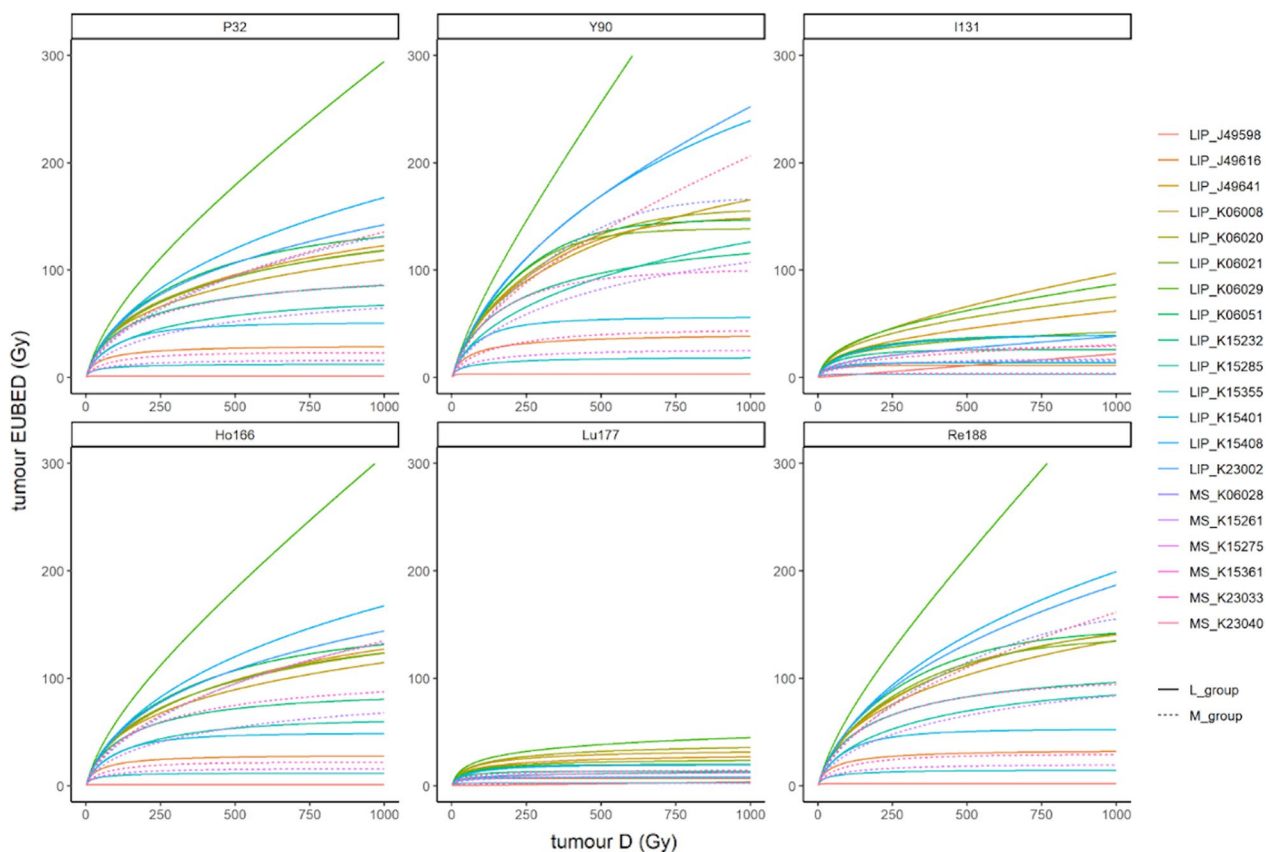


Fig. 6 Tumor EUBED in Gy as a function of tumor-absorbed dose *D* in Gy for ³²P, ⁹⁰Y, ¹³¹I, ¹⁶⁶Ho, ¹⁷⁷Lu, and ¹⁸⁸Re

Aside from these differences, the Lipiodol® ultra-fluid does not remain in the healthy liver parenchyma [13, 31, 32] contrary to microspheres that are blocked by microvessels, regardless of being tumoral or healthy tissue feeders. This could be an advantage for Lipiodol® ultra-fluid as a radionuclide carrier for radioembolization treatments where more than a single segment of the liver needs to be treated. Different retention mechanisms are currently evoked in the tumor (accumulation of the product in the peri-tumoral sinuses by an embolization mechanism [27], modification of the membrane potential or of the permeability of the tumor vessels [31], slower elimination linked to a deficiency in Kupffer cells and lymphatic vessels in the tumor, membrane and then intra-cellular fixation, pinocytosis of Lipiodol® ultra-fluid droplets in HepG2 cells). While the microspheres remain blocked in the microvessels with heterogeneity in targeting the tumor, the slow infusion of radiolabeled Lipiodol® ultra-fluid in the tumor may offer potential for better biological effectiveness while preserving the healthy liver tissues.

This study clearly shows that there are some trends toward a better penetration of Lipiodol® ultra-fluid that

may translate into a better radiation efficacy. The comparison of various radionuclides on such a dataset had never been done before. One interesting result is that at an absorbed dose of 100 Gy, the greatest simulated biological efficacy was obtained with ⁹⁰Y and ¹⁸⁸Re, while the lowest was obtained for ¹³¹I and ¹⁷⁷Lu. This can be explained by the longest beta radiation range of ⁹⁰Y and ¹⁸⁸Re, but also their shortest half-life resulting in a higher dose-rate for a given absorbed dose delivered. Indeed, at higher dose-rate, the cell-killing effect is higher due to lack of reparation capabilities. In between, we found ³²P, ¹⁶⁶Ho, whose EUBED values are not statistically different but remain one-third below those of ⁹⁰Y.

Our study has several limitations. First, the number of animals differ between groups and the imaging points are not equal in each group. This is due to the primary endpoint, which was to study the biodistribution kinetic of Lipiodol® ultra-fluid in VX2 tumors, which limits the interpretation of these results. Another limitation is the choice of model since there is no HCC model in rabbits. Nevertheless, although not of hepatic origin, the VX2 model is commonly used as an alternative for interventional radiotherapy studies [33].

Table 3 EUBED in Gy for $D=100$ Gy values for the L and M groups and following radionuclides: ^{32}P , ^{90}Y , ^{131}I , ^{166}Ho , ^{177}Lu , ^{188}Re

	EUBED (Gy) for $D=100$ Gy					
	^{32}P	^{90}Y	^{131}I	^{166}Ho	^{177}Lu	^{188}Re
LIP_J49598	1.47	3.42	2.30	0.99	0.39	1.74
LIP_J49616	20.0	24.9	9.81	19.7	6.48	21.8
LIP_J49641	43.8	53.7	23.2	43.6	16.9	47.7
LIP_K06008	43.4	54.1	29.2	43.8	19.6	47.8
LIP_K06020	45.6	55.2	27.5	45.4	20.6	49.2
LIP_K06021	44.0	56.9	20.8	44.0	16.1	48.9
LIP_K06029	59.3	70.9	30.3	58.9	23.7	63.9
LIP_K06051	47.9	57.9	22.6	47.2	14.8	51.6
LIP_K15232	40.7	48.9	18.3	39.9	11.1	43.7
LIP_K15285	30.4	39.6	10.9	29.4	7.05	33.7
LIP_K15355	9.45	12.5	3.07	9.27	2.37	10.6
LIP_K15401	30.7	36.3	11.4	29.8	6.83	32.7
LIP_K15408	47.8	59.1	21.1	47.1	13.6	51.9
LIP_K23002	46.5	60.3	14.3	45.8	8.13	51.7
Mean \pm sd	36.5 \pm 16	45.3 \pm 20	17.5 \pm 9	36.1 \pm 16	12.0 \pm 7	39.8 \pm 18
MS_K06028	36.6	49.2	10.3	36.3	6.43	41.4
MS_K15261	25.6	35.3	9.43	26.0	5.90	29.5
MS_K15275	10.8	15.6	3.20	10.9	1.99	12.6
MS_K15361	38.6	48.4	15.0	38.4	9.65	42.4
MS_K23033	15.2	23.0	3.27	14.8	1.95	17.8
MS_K23040	38.8	48.8	12.5	38.2	7.67	42.3
Mean \pm sd	27.6 \pm 12	36.7 \pm 15	8.96 \pm 4.8	27.4 \pm 12	5.60 \pm 3.0	31.0 \pm 13
Wilcoxon p	0.11	0.13	0.08	0.11	0.04	0.11

Wilcoxon p values were calculated for each radionuclide between the L and M groups, with the hypothesis of L values greater than M

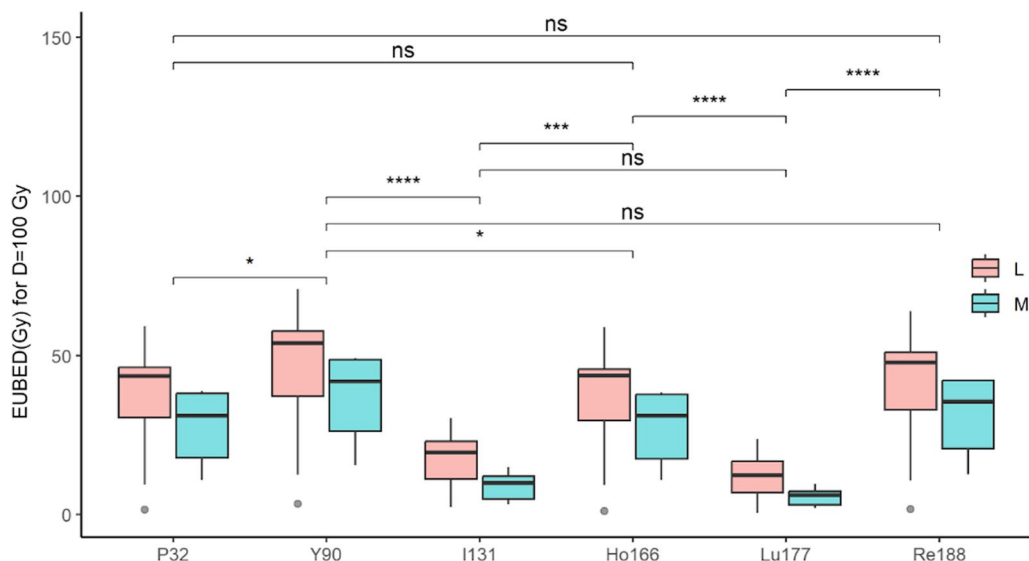


Fig. 7 EUBED in Gy for $D=100$ Gy values presented as boxplots for the L and M groups, for ^{32}P , ^{90}Y , ^{131}I , ^{166}Ho , ^{177}Lu , and ^{188}Re . * indicates the difference is significant, while ns indicates it is non-significant

Conclusion

The aim of this study was to compare the ability of Lipiodol® ultra-fluid and microspheres to target the tumor tissues for radioembolization purposes. The images obtained from μ CT on ex vivo tumors have demonstrated the ability of Lipiodol® ultra-fluid to penetrate the tumor more extensively than the microspheres and confirm that Lipiodol® ultra-fluid remains in the tumor compartment for at least 12 days. This ability translated into a higher simulated EUBED than for microspheres, hence the potential of Lipiodol® ultra-fluid for a better efficacy. This study allowed also to confirm that ^{90}Y might be the best candidate radionuclide for radioembolization, either with Lipiodol® ultra-fluid or microspheres, in terms of efficacy, but ^{32}P , ^{166}Ho , and ^{188}Re can achieve close results, contrary to ^{131}I and ^{177}Lu . The results of this study could be used to investigate the development of novel radioembolization agents with Lipiodol® ultra-fluid as a radioactivity delivery agent and to help transposing the clinical results from an agent to another.

Abbreviations

3D	Tri-dimensional
BCLC	Barcelona Clinic Liver Cancer
BED	Biological effective dose
CSDA	Continuous slowing-down approximation
DPK	Dose-point kernel
EUD	Equivalent uniform dose
EUBED	Equivalent uniform biological effective dose
HCC	Hepatocellular carcinoma
MIRD	Medical internal radiation dose
μ CT	Micro-computerized tomography
SSS	Super-six sulfur

Supplementary Information

The online version contains supplementary material available at <https://doi.org/10.1186/s13550-023-01051-9>.

Additional file 1. Supplemental data: boxplots and correlation maps of the radiomic analysis, and absorbed dose estimations tabulated and represented as dose-volume histograms.

Acknowledgements

Not applicable.

Author contributions

AD, SB, PV and RS contributed to the study conception and design. Material preparation, data collection and analysis were performed by AD, MS, CH, MCDG and RS. The first draft of the manuscript was written by AD. SB and RS commented on previous versions of the manuscript. All authors read and approved the final manuscript.

Funding

This work was funded by Guerbet France.

Availability of data and materials

All data generated or analyzed during this study are included in this published article and its supplementary files.

Declarations

Ethics approval and consent to participate

All animal experiments were conducted in compliance either with the ARRIVE guidelines. The protocol was approved by the local research ethics committee of Guerbet France and authorized by the French Ministry of Higher education and Research (APAFIS#4592).

Consent for publication

Not applicable.

Competing interests

AD has received payment for lectures, including service on speaker's bureaus, from Sirtex; received payment for board membership from Boston Scientific. MS, CH, MCDG and RS are employees of Guerbet France.

Received: 13 September 2023 Accepted: 8 November 2023

Published online: 23 November 2023

References

- Sung H, et al. Global cancer statistics 2020: GLOBOCAN estimates of incidence and mortality worldwide for 36 Cancers in 185 countries. *CA Cancer J Clin*. 2021;71(3):209–49. <https://doi.org/10.3322/caac.21660>.
- Reig M, et al. BCLC strategy for prognosis prediction and treatment recommendation: the 2022 update. *J Hepatol*. 2022;76(3):681–93. <https://doi.org/10.1016/j.jhep.2021.11.018>.
- Pasciak AS, et al. The number of microspheres in Y90 radioembolization directly affects normal tissue radiation exposure. *Eur J Nucl Med Mol Imaging*. 2020;47:816–27. <https://doi.org/10.1007/s00259-019-04588-x>.
- d'Abadie P, et al. Accurate non-tumoral ^{99m}Tc -MAA absorbed dose prediction to plan optimized activities in liver radioembolization using resin microspheres. *Phys Med*. 2021;89:250–7. <https://doi.org/10.1016/j.ejmp.2021.07.032>.
- Walrand S, Hesse M, Jamar F, Lhomme R. A hepatic dose-toxicity model opening the way toward individualized radioembolization planning. *J Nucl Med*. 2014;55(8):1317–22. <https://doi.org/10.2967/jnumed.113.135301>.
- Romanò C, et al. Radioembolization of hepatocellular carcinoma with ^{90}Y glass microspheres: no advantage of voxel dosimetry with respect to mean dose in dose-response analysis with two radiological methods. *Cancers*. 2022;14(4):959. <https://doi.org/10.3390/cancers14040959>.
- Kobayashi H, Nakajo M, Yano T, Shimabukuro K, Shinohara S. Transcatheter internal radiotherapy of hepatoma using radioactive iodized oil (^{131}I Lipiodol). *Nihon Igaku Hoshasen Gakkai Zasshi Nippon Acta Radiol*. 1985;45(8):1176–8.
- Raoul JL, Bourguet P, Bretagne JF. Hepatic Artery injection of I-131-labeled Lipiodol part I. Biodistribution study results in patients with hepatocarcinoma and liver metastases. *Radiology*. 1988;168(2):541–5.
- Lepareur N, Ardisson V, Noiret N, Garin E. (188)Re-SSS/Lipiodol: development of a potential treatment for HCC from bench to bedside. *Int J Mol Imaging*. 2012;2012:278–306. <https://doi.org/10.1155/2012/278306>.
- Konno T, et al. Effect of arterial administration of high-molecular-weight anticancer agent SMANCS with lipid lymphographic agent on hepatoma: a preliminary report. *Eur J Cancer Clin Oncol*. 1983;19(8):1053–65. [https://doi.org/10.1016/0277-5379\(83\)90028-7](https://doi.org/10.1016/0277-5379(83)90028-7).
- Konno T, et al. Selective targeting of anti-cancer drug and simultaneous image enhancement in solid tumors by arterially administered lipid contrast medium. *Cancer*. 1984;54(11):2367–74. [https://doi.org/10.1002/1097-0142\(19841201\)54:11%3c2367-74::AID-CNCR2820541111%3e3.0.CO;2-F](https://doi.org/10.1002/1097-0142(19841201)54:11%3c2367-74::AID-CNCR2820541111%3e3.0.CO;2-F).
- Folkman J. Tumor angiogenesis. In: *Advances in cancer research*. Elsevier, 1974, pp. 331–358. [https://doi.org/10.1016/S0065-230X\(08\)60058-5](https://doi.org/10.1016/S0065-230X(08)60058-5).
- Iwai K, Maeda H, Konno T. Use of oily contrast medium for selective drug targeting to tumor: enhanced therapeutic effect and X-ray image. *Cancer Res*. 1984;44(5):2115–21.
- Konno T. Targeting chemotherapy for hepatoma: Arterial administration of anticancer drugs dissolved in lipiodol. *Eur J Cancer*. 1992;28(2):403–9. [https://doi.org/10.1016/S0959-8049\(05\)80063-2](https://doi.org/10.1016/S0959-8049(05)80063-2).

15. Bouvry C, et al. Transarterial radioembolization (TARE) agents beyond 90 Y-microspheres. *BioMed Res Int*. 2018;2018:1–14. <https://doi.org/10.1155/2018/1435302>.
16. Eckerman KF, Endo A. MIRD: radionuclide data and decay schemes. In: Society of Nuclear Medicine, vol. 50. Society of Nuclear Medicine, 2007. Available: <http://www.worldcat.org/title/mird-radionuclide-date-and-decay-schemes/oclc/612052780>
17. Seltzer S. Stopping-powers and range tables for electrons, protons, and helium ions, NIST standard reference database 124. *Nat Inst Stand Technol*. 1993. <https://doi.org/10.18434/T4NC7P>.
18. Pascale F, et al. Rabbit VX2 liver tumor model: a review of clinical, biology, histology, and tumor microenvironment characteristics. *Front Oncol*. 2022;12:871829. <https://doi.org/10.3389/fonc.2022.871829>.
19. Fedorov A, et al. 3D slicer as an image computing platform for the quantitative imaging network. *Magn Reson Imaging*. 2012;30(9):1323–41. <https://doi.org/10.1016/j.mri.2012.05.001>.
20. van Griethuysen JJM, et al. Computational radiomics system to decode the radiographic phenotype. *Cancer Res*. 2017;77(21):e104–7. <https://doi.org/10.1158/0008-5472.CAN-17-0339>.
21. Sanchez-Garcia M, Gardin I, Lebtahi R, Dieudonné A. A new approach for dose calculation in targeted radionuclide therapy (TRT) based on collapsed cone superposition: validation with (90)Y. *Phys Med Biol*. 2014;59(17):4769–84. <https://doi.org/10.1088/0031-9155/59/17/4769>.
22. Sanchez-Garcia M, Gardin I, Lebtahi R, Dieudonné A. Implementation and validation of collapsed cone superposition for radiopharmaceutical dosimetry of photon emitters. *Phys Med Biol*. 2015;60(20):7861–76. <https://doi.org/10.1088/0031-9155/60/20/7861>.
23. Bolch WE, Eckerman KF, Sgouros G, Thomas SR. MIRD pamphlet No. 21: a generalized schema for radiopharmaceutical dosimetry—standardization of nomenclature. *J Nucl Med*. 2009;50(3):477–84. <https://doi.org/10.2967/jnumed.108.056036>.
24. Strigari L, et al. Efficacy and toxicity related to treatment of hepatocellular carcinoma with 90Y-SiR spheres: radiobiologic considerations. *J Nucl Med*. 2010;51(9):1377–85. <https://doi.org/10.2967/jnumed.110.075861>.
25. Cremonesi M, et al. Radioembolization of hepatic lesions from a radiobiology and dosimetric perspective. *Front Oncol*. 2014;4:1–20. <https://doi.org/10.3389/fonc.2014.00210>.
26. van Leeuwen CM, et al. The alfa and beta of tumours: a review of parameters of the linear-quadratic model, derived from clinical radiotherapy studies. *Radiat Oncol*. 2018;13(1):96. <https://doi.org/10.1186/s13014-018-1040-z>.
27. Jones LC, Hoban PW. Treatment plan comparison using equivalent uniform biologically effective dose (EUBED). *Phys Med Biol*. 2000;45(1):159–70. <https://doi.org/10.1088/0031-9155/45/1/311>.
28. Posit Team. RStudio: integrated development environment for R. Posit Software, Boston, MA, PBC, 2022. Available: <http://www.posit.co/>
29. R Core Team. R: a language and environment for statistical computing. R Foundation for Statistical Computing, Vienna, Austria, 2022. Available: <https://www.R-project.org/>
30. Weber M, et al. EANM procedure guideline for the treatment of liver cancer and liver metastases with intra-arterial radioactive compounds. *Eur J Nucl Med Mol Imaging*. 2022;49(5):1682–99. <https://doi.org/10.1007/s00259-021-05600-z>.
31. Nakakuma K, et al. Studies on anticancer treatment with an oily anticancer drug injected into the ligated feeding hepatic artery for liver cancer. *Cancer*. 1983;52(12):2193–200. [https://doi.org/10.1002/1097-0142\(19831215\)52:12%3c2193::AID-CNCR2820521203%3e3.0.CO;2-R](https://doi.org/10.1002/1097-0142(19831215)52:12%3c2193::AID-CNCR2820521203%3e3.0.CO;2-R).
32. Becker S, et al. Optimization of hepatocarcinoma uptake with radiolabeled lipiodol: development of new lipiodol formulations with increased viscosity. *Cancer Biother Radiopharm*. 2012;27(2):149–55. <https://doi.org/10.1089/cbr.2011.1072>.
33. Chandra VM, Wilkins LR, Brautigan DL. Animal models of hepatocellular carcinoma for local-regional intraarterial therapies. *Radiol Imaging Cancer*. 2022;4(4):e210098. <https://doi.org/10.1148/rycan.210098>.

Publisher's Note

Springer Nature remains neutral with regard to jurisdictional claims in published maps and institutional affiliations.

Submit your manuscript to a SpringerOpen® journal and benefit from:

- Convenient online submission
- Rigorous peer review
- Open access: articles freely available online
- High visibility within the field
- Retaining the copyright to your article

Submit your next manuscript at ► [springeropen.com](https://www.springeropen.com)
